arXiv:1603.00499v2 [physics.comp-ph] 3 Mar 2016

A Computational Method to Calculate the Exact Solution for Acoustic Scattering by Liquid Spheroids

Edmundo Lavia, Juan D. Gonzalez, Silvia Blanc

March 4, 2016

Abstract

The problem of scattering of harmonic plane acoustic waves by liquid spheroids (prolate and oblate) is addressed from an analytical approach. Mathematically, it consists in solving the Helmholtz equation in an unbounded domain with Sommerfeld radiation condition at infinity. The domain where propagation takes place is characterised by density and sound speed values ρ_0 and c_0, respectively, while ρ_1 and c_1 are the corresponding density and sound speed values of an inmersed object that is responsible of the scattered field. Since Helmholtz equation is separable in prolate (oblate) spheroidal coordinates, its exact solution for the scattered field can be expressed as an expansion on prolate (oblate) spheroidal functions multiplied by coefficients whose values depend upon the boundary conditions verified at the medium-inmersed fluid obstacle interface. The general case ($c_0 \neq c_1$) is cumbersome and it has only been theoretically calculated. In this paper, a numerical implementation of the general exact solution that is valid for any range of eccentricity values and for $c_0 \neq c_1$, is provided. The high level resolutor layer code has been written in the Julia programming language. A software package recently released in the literature has been used to compute the spheroidal functions. Several limiting cases (Dirichlet and Neumann boundary conditions, spheroid tending to sphere) have been satisfactorily evaluated using the implemented code. The numerical implementation of the exact solution leads to results that are in agreement with reported predicted results obtained through approximate solutions for far-field and near-field regimes. The example scripts shown here can be downloaded from authors' web (GitHub) site.

1 Introduction

The interaction of harmonic plane sound waves with spheroids (prolate and oblate) has been widely and increasingly investigated, mainly for soft and rigid scatterers, along the last six decades in different branches of acoustics [1, 2, 3]. In particular, underwater acoustics can be considered quite proliferous in reported articles on different aspects of this topic due to its relevance in applications to fisheries management and marine ecosystem research.

Many developed models provide exact or approximate solutions with harmonic time dependence for the general problem of acoustic scattering by spheroids which have been extensively applied to several aquatic organisms and objects inmersed in the ocean [4, 5, 6]. Both for soft and rigid scatterers, computational implementations of approximate solutions have been published for either near or far-field conditions.

However, less attention has received the case of liquid spheroidal scatterers till 1964 when the corresponding analytical solution for the oblate case was published for the first time [7]. Three years later numerically computed results of the scattered wave radiation

patterns were reported only for a particular case of sound speed ratio, $c_0/c_1 = 1$, being c_0 and c_1 are the sound speed in the medium and the fluid prolate spheroid, respectively [8]. In 1988 Furusawa [4] numerically computed an approximate solution for the acoustic backscattering patterns by liquid prolate spheroids for specific cases when the sound speed and density ratios verify $c_0/c_1 \approx 1$ and $\rho_0/\rho_1 \approx 1$. Several authors have used approximate solutions in the last years [9, 10]. More recently, another reference [11] considers the general case $c_0 \neq c_1$ and $\rho_0 \neq \rho_1$ but only for spheroids with low eccentricity. In contrast with such quite widespread approximate solutions, this paper addresses an analytical approach; it provides a numerical implementation of an exact solution for a liquid spheroidal scatterer.

Mathematically, the problem of acoustic scattering of plane waves with harmonic dependence consists in solving Helmholtz equation in an unbounded domain with Sommerfeld radiation condition at infinity. The domain where propagation takes place is characterised by density and sound speed values ρ_0 and c_0, respectively, while ρ_1 and c_1 are the corresponding density and sound speed values of an object inmersed in that medium that is responsible of the scattered field. Different boundary conditions must be verified for the medium-object interface according to the type of scatterrer considered, namely, gas-filled (Dirichlet's boundary conditions), rigid (Neumann b.c.) or liquid. The solution of the scalar wave equation strongly depends on the object's shape and there exist exact solutions only for a few cases. When the object is a sphere, the canonical case, the exact solution is based on an expansion in spherical wave functions [12]. For scatterers of spheroidal shape, the exact solution can be expanded on prolate (or oblate) spheroidal wave functions as a result of applying separation of variables to Helmholtz equation expressed in spheroidal coordinates [13, 14].

As far as the authors are aware, for the first time in this paper a new computer implementation based on the exact solution for liquid spheroids valid for any value of eccentricity and arbitrary c_0, c_1, ρ_0, ρ_1, is provided. The implementation of this solution was developed using recently available computational code by Adelman et al. [15] (which will be called AGD software from now on) together with a high level layer code implemented in the Julia programming language [16].

As it is well known, for many cases of interest (e.g. $ka \gg 1$, being k the wave number and a a typical longitudinal dimension of the scatterer) computation of spheroidal wave functions requires precision beyond the one provided by hardware floating point numbers [17](currently 64 bits in the consumer market). In fact, the AGD code implements floating point arbitrary precision through the use of a specialized C++ library. The Julia language is a relatively new free programming language with some features that make it especially attractive for the implementation of the spheroidal wave function related code, that is the possibility of having floating point arbitrary precision arithmetic and algebra, both features built in *right out of the box*. On the other hand, its calculation speed compared to other high-level equivalent computational environments constitutes a very advantageous feature.

This paper is structured as follows. In Section 2 the analytical exact solution is rederived. Basically, it is a refurbished derivation that closely follows the previous work by Yeh [7] but contemplating both cases, prolate and oblate, and correcting some minor typos. This section provides the basis for subsequent formulation and establishes the nomenclature that is used in the whole article. Section 3 is the core of the work, namely, the algorithmic procedure of the coefficient's calculation. Section 4 shows far-field patterns in the limiting cases when the liquid solution tends to the Dirichlet and Neumann solution and when the spheroid tends to sphere. Computations of near-field are also carried out. On the other hand, a comparison with previous published results is made. In Section 5,

the computational implementation of the numerical solution under the Julia idiosincracy is described as well as a brief explanation on the sintaxis of the presented computational code is given. Finally, the conclusions of the work are summarized in Section 6.

2 Analytical exact solution

When acoustic scattering by spheroids is considered, it is convenient to use a spheroidal curvilinear coordinate system (ξ, η, φ) [13]. The relationship between the prolate spheroidal coordinates and the Cartesian coordinates, is given by the following transformation [15]:

$$\begin{cases} x = \dfrac{d}{2}\,\left[(\xi^2-1)\,(1-\eta^2)\right]^{1/2}\,\cos\varphi \\ \\ y = \dfrac{d}{2}\,\left[(\xi^2-1)\,(1-\eta^2)\right]^{1/2}\,\sin\varphi \\ \\ z = \dfrac{d}{2}\,\xi\,\eta, \end{cases}$$

where d is the interfocal distance of the ellipse of major semi-axis $a = (d/2)\,\xi$ and minor semi-axis $b = (d/2)\,(\xi^2-1)^{1/2}$ (See Figure 1). The values for the three prolate spherical coordinates must lie between the following bounds:

$$1 \leq \xi, \quad -1 \leq \eta \leq 1, \quad 0 \leq \varphi < 2\pi.$$

The prolate spheroidal coordinate ξ-range of variation is directly associated with the shape of the spheroid, ranging from $\xi = 1$ (corresponding to the segment of length d between both spheroid foci) to ξ tending to ∞ (corresponding to a sphere of radius $a = b$). The surface of the prolate spheroid coincides with the coordinate surface given by equation $\xi = \xi_0$, with $\xi_0 = (1-(b/a)^2)^{-1/2}$ and $d = 2(a^2-b^2)^{1/2}$.

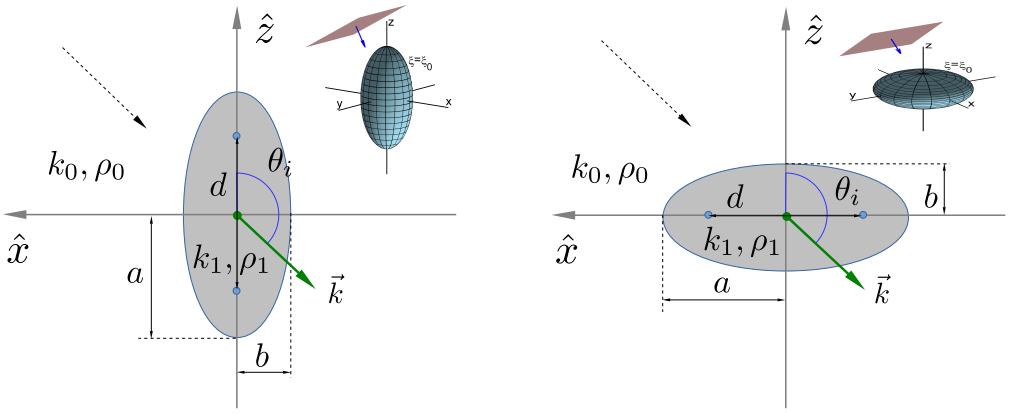

Figure 1: Prolate (left) and oblate (right) coordinate system and related conventions.

On the other hand, the relationship for oblate spheroidal coordinates is given by

$$\begin{cases} x = \dfrac{d}{2}\,\left[(\xi^2+1)\,(1-\eta^2)\right]^{1/2}\,\cos\varphi \\ \\ y = \dfrac{d}{2}\,\left[(\xi^2+1)\,(1-\eta^2)\right]^{1/2}\,\sin\varphi \\ \\ z = \dfrac{d}{2}\,\xi\,\eta, \end{cases}$$

where coordinates ranges are

$$\xi \geq 0 \ , \quad -1 \leq \eta \leq 1 \ , \quad 0 \leq \varphi < 2\pi \ ,$$

and the surface of the oblate spheroid coincides with the coordinate surface given by equation $\xi = \xi_0$ where $\xi_0 = ((a/b)^2 - 1)^{-1/2}$.

For harmonic wave fields propagating in an unbounded medium, the acoustic pressure exterior and interior to a prolate (oblate) spheroidal surface of a liquid scatterer inmersed in that medium is governed by Helmholtz equation

$$\nabla^2 p + k^2 p = 0,$$

which is separable in prolate (oblate) spheroidal coordinates. Thus, the problem of solving a partial differential equation in an unbounded domain with the Sommerfeld radiation at infinity is reduced to solving two ordinary differential equations for radial and angular prolate (oblate) spheroidal functions, $R(\xi)$ and $S(\eta)$, respectively [1, 7, 15, 18].

At this point is worth noting that letting

$$\xi \to i\xi \qquad \text{and} \qquad h_0 = (d/2)k_0 \to -ih_0, \tag{1}$$

provides a direct transformation from the prolate to the oblate case [15, 18]. their corresponding solutions to the oblate respective ones [15, 18]. Therefore, from now on all mathematical expressions are valid for the liquid prolate spheroid and can be easily transformed to the oblate spheroid through the given conversion rule.

An incident plane acoustic wave on a prolate (oblate) spheroid, with angular frequency ω and wave number $k_0 = \omega/c_0$, is schematically illustrated in Figure 1, including both prolate and oblate coordinate systems used in this paper.

Without loss of generality, due to the simmetry of revolution around the z axis, the acoustic pressure corresponding to an incident plane wave can be written as

$$p_i = p_0 \exp(i\vec{k_0} \cdot \vec{r}),$$

where $\vec{k_0} = k_0(\sin\theta_i, 0, \cos\theta_i)$, the amplitude p_0 is a real number and θ_i is the incident angle measured as indicated in Figure 1. This expression can be expanded on prolate spheroidal functions [19] so that at an arbitrary field point $\vec{r} = \vec{r}(\xi, \eta, \varphi)$,

$$p_i(\vec{r}) = 2p_0 \sum_{m\geq 0} \sum_{n\geq m} i^n \frac{\epsilon_m}{N_{mn}} \, S_{mn}(h_0, \cos(\theta_i)) \, S_{mn}(h_0, \eta) \, R^{(1)}_{mn}(h_0, \xi) \cos(m\varphi) \tag{2}$$

where the subscripts m, n are natural numbers, S_{mn} are the angular spheroidal wave functions, $R^{(1)}_{mn}$ are the radial spheroidal wave functions of first kind, i is the imaginary complex unit ($i^2 = -1$), ϵ_m is the Neumann factor, defined as $\epsilon_m = 2$ if $m \neq 0$ and $\epsilon_m = 1$ if $m = 0$, the parameter h_0 is defined as $h_0 = (d/2)k_0$ and N_{mn} are the norms, given by

$$N_{mn} = \int_{-1}^{1} S^2_{mn}(h_0, \eta) \, d\eta.$$

The analytical solutions for the scattered and transmitted acoustic pressure, $p_s(\vec{r})$ and $p_t(\vec{r})$, respectively, can be expressed as,

$$p_s(\vec{r}) = 2p_0 \sum_{m\geq 0} \sum_{n\geq m} i^n A_{mn} \frac{\epsilon_m}{N_{mn}} \, S_{mn}(h_0, \cos(\theta_i)) \, S_{mn}(h_0, \eta) \, R^{(3)}_{mn}(h_0, \xi) \, \cos(m\varphi), \tag{3}$$

$$p_t(\vec{r}) = 2p_0 \sum_{m\geq 0} \sum_{n\geq m} i^n B_{mn} \frac{\epsilon_m}{N_{mn}} S_{mn}(h_0, \cos(\theta_i))\, S_{mn}(h_1, \eta)\, R^{(1)}_{mn}(h_1, \xi)\, \cos(m\varphi). \quad (4)$$

The subscripts 0 and 1 (see Figure 1) refers to the surrounding medium and to the interior of the prolate spheroidal liquid obstacle, respectively, and A_{mn} and B_{mn} are the unknown expansion coefficients. Precisely, the key point of this work, is to determine them applying appropriate boundary conditions at the medium-inmersed liquid spheroid interface, that means to apply for the continuity of the pressure and the normal component of media particle velocity at the boundary, given by $\xi = \xi_0$. In symbols,

$$(p_i + p_s)|_{\xi=\xi_0} = p_t|_{\xi=\xi_0} \quad (5)$$

$$\frac{1}{\rho_0} \left.\frac{\partial(p_i + p_s)}{\partial \xi}\right|_{\xi=\xi_0} = \frac{1}{\rho_1} \left.\frac{\partial p_t}{\partial \xi}\right|_{\xi=\xi_0}. \quad (6)$$

With the purpose of enabling the computation of the A_{mn} and B_{mn} coefficients, included in Equations (3) and (4), it is convenient to expand $S_{mn}(h_0, \eta)$ in terms of $\{S_{m\ell}(h_1, \eta)\}$

$$S_{mn}(h_0, \eta) = \sum_{\ell=m}^{\infty} \alpha^{(m)}_{n\ell} S_{m\ell}(h_1, \eta), \quad (7)$$

where

$$\alpha^{(m)}_{n\ell} = \frac{\int_{-1}^{1} S_{mn}(h_0, \eta) S_{m\ell}(h_1, \eta) d\eta}{\int_{-1}^{1} S^2_{m\ell}(h_1, \eta) d\eta}.$$

Substituting of Equation (7) in the left-hand side of Equations (5) and (6) and using the orthogonality properties of the family $\{S_{mn}(h_1, \eta)\cos(m\varphi) : m \geq 0, n \geq m\}$ lead to a matricial system involving the A_{mn} and B_{mn} coefficients.

Defining the $Q^{(m)}_{n\ell}$ matrix and $f^{(m)}_{\ell}$ as

$$Q^{(m)}_{n\ell} = i^n \frac{1}{N_{mn}} \alpha^{(m)}_{n\ell}\, S_{mn}(h_0, \cos(\theta_i)) \left[\frac{\rho_1}{\rho_0} \frac{R^{(3)\prime}_{mn}(h_0, \xi_0) R^{(1)}_{m\ell}(h_1, \xi_0)}{R^{(1)\prime}_{m\ell}(h_1, \xi_0)} - R^{(3)}_{mn}(h_0, \xi_0)\right],$$

$$f^{(m)}_{\ell} = -\sum_{n=0}^{\infty} i^n \frac{1}{N_{mn}} \alpha^{(m)}_{n\ell}\, S_{mn}(h_0, \cos(\theta_i)) \left[\frac{\rho_1}{\rho_0} \frac{R^{(1)\prime}_{mn}(h_0, \xi_0) R^{(1)}_{m\ell}(h_1, \xi_0)}{R^{(1)\prime}_{m\ell}(h_1, \xi_0)} - R^{(1)}_{mn}(h_0, \xi_0)\right],$$

where the ξ derivative is indicated with a prime (i.e. $' \equiv d/d\xi$), it can be shown that the A_{mn}, with $(n = m, m+1, ..)$, verify

$$\sum_{n=m}^{\infty} A^{(m)}_n Q^{(m)}_{n\ell} = f^{(m)}_{\ell} \qquad \ell = m, m+1, ... \quad (8)$$

where m is indicated as superscript to emphasize the fact that for each fixed m, the left hand side of Equation (8) is a standard product of a row vector $(A^{(m)}_m, A^{(m)}_{m+1}, \ldots, A^{(m)}_n, \ldots)$ and a matrix $Q^{(m)}_{n\ell}$ while the right side is a row indexed by ℓ. For each $m = 1, 2, ...$, the system (8) can be solved with standard and well known computational algebra tricks as it is shown in the next section.

After having computed the A_{mn}, it follows that the other coefficients B_{mn}, associated to the transmitted waves, can also be calculated as

$$B_{m\ell} = \sum_{n=m}^{\infty} i^{n-\ell} \frac{N_{m\ell}}{N_{mn}} \alpha^{(m)}_{n\ell} \frac{S_{mn}(h_0, \cos(\theta_i))}{S_{m\ell}(h_0, \cos(\theta_i))} \left[\frac{R^{(1)}_{mn}(h_0, \xi_0) + A_{mn}\, R^{(3)}_{mn}(h_0, \xi_0)}{R^{(1)}_{m\ell}(h_1, \xi_0)}\right]. \quad (9)$$

In the far-field limit it can be shown [7] that

$$p_s(r,\theta,\varphi) \approx p_0 \frac{e^{ik_0 r}}{r} f_\infty(\theta,\varphi),$$

where r, θ, φ are the spherical polar coordinates of the observation point and

$$f_\infty(\theta,\varphi) = \frac{2}{ik_0} \sum_{\substack{m\geq 0 \\ n\geq m}} A_{mn} \frac{\epsilon_m}{N_{mn}} \, S_{mn}(h_0, \cos(\theta_i)) \, S_{mn}(h_0, \cos(\theta)) \cos(m\varphi)$$

is the so called far-field scattering amplitude function which is widespread used in different acoustic scattering applications.

3 Algorithmic procedure

The numerical computation of the A_{mn} and B_{mn} coefficients starts with a truncation procedure. The series in Equation (8) is truncated at M, so that for each value of m, there are $M - m + 1$ unknown $A_n^{(m)}$, where index n takes natural values in the interval $[m, M]$. Thus, $A_n^{(m)}$ satisfies the linear system

$$\sum_{n=m}^{M} A_n^{(m)} Q_{n\ell}^{(m)} = f_\ell^{(m)} \qquad \ell = m, m+1, .., M \tag{10}$$

where $A^{(m)}$ and $f^{(m)}$ are row arrays $\in \mathbb{C}^{1\times(M-m+1)}$ and $Q^{(m)}$ is a matrix $\in \mathbb{C}^{(M-m+1)\times(M-m+1)}$.

The successive matricial systems obtained as a consequence of truncation, Equation (10), are

- for $m = 0$,

$$\left(A_0^{(0)}, A_1^{(0)}, .., A_M^{(0)}\right) \begin{pmatrix} Q_{0,0}^{(0)} & Q_{0,1}^{(0)} & \cdots & Q_{0,M}^{(0)} \\ Q_{1,0}^{(0)} & Q_{1,1}^{(0)} & \cdots & Q_{1,M}^{(0)} \\ \vdots & \vdots & \ddots & \vdots \\ Q_{M,0}^{(0)} & Q_{M,1}^{(0)} & \cdots & Q_{M,M}^{(0)} \end{pmatrix} = \left(f_0^{(0)}, f_1^{(0)}, .., f_M^{(0)}\right) \tag{11}$$

- for $m = 1$,

$$\left(A_1^{(1)}, A_2^{(1)}, .., A_M^{(1)}\right) \begin{pmatrix} Q_{1,1}^{(1)} & Q_{1,2}^{(1)} & \cdots & Q_{1,M}^{(1)} \\ Q_{2,1}^{(1)} & Q_{2,2}^{(1)} & \cdots & Q_{2,M}^{(1)} \\ \vdots & \vdots & \ddots & \vdots \\ Q_{M,1}^{(1)} & Q_{M,2}^{(1)} & \cdots & Q_{M,M}^{(1)} \end{pmatrix} = \left(f_1^{(1)}, f_2^{(1)}, .., f_M^{(1)}\right) \tag{12}$$

- ...

- for $m = M - 1$,

$$\left(A_{M-1}^{(M-1)}, A_M^{M-1}\right) \begin{pmatrix} Q_{M-1,M-1}^{(M-1)} & Q_{M-1,M}^{(M-1)} \\ Q_{M,M-1}^{(M-1)} & Q_{M,M}^{(M-1)} \end{pmatrix} = \left(f_{(M-1)}^{(M-1)}, f_M^{(M-1)}\right) \tag{13}$$

- and finally, for $m = M$,

$$A_M^{(M)} Q_{M,M}^{(M)} = f_M^{(M)}.$$

In summary, the algorithm calculates the $Q^{(m)}$ matrix and $f^{(m)}$ array using the AGD software at each step (indexed by m) and solves each linear system induced by them at the Julia layer level in order to get the $A_n^{(m)}$ coefficients. Then, the $B_n^{(m)}$ coefficients are easily calculated from Equation (9).

4 Numerical results

4.1 Verification for extreme cases in the far-field approximation

Algorithm verification was conducted via evaluation of the exact solution for $|f_\infty|$, obtained through the implemented codes for a liquid prolate (oblate) spheroidal scatterer, against known results valid in some extreme cases (such as spheroid tending to a sphere, Dirichlet and Neumann boundary conditions at the medium-spheroid interface).

A liquid spheroid approaching a sphere, with major semi-axis $a = 1$ and minor semi-axis $b = 0.99$, is assumed in order to compare the results predicted by the implemented codes with the classical solution for plane wave acoustic scattering by a liquid sphere [20]. Two different incident directions are considered, given by the line that contains both focis of an oblate spheroid (i.e. $\hat{x}$ incidence) and of a prolate spheroid (i.e. $\hat{z}$ incidence), in agreement with the coordinate system shown in Figure 1. The sphere has a reference radius $a = 1$. Calculations were made for $k_0 = 5, k_1 = 3, \rho_1/\rho_0 = 3$. Plottings of the scattering patterns obtained with the implemented numerical codes for liquid prolate and oblate spheroidal scatterer tending to coincide with the corresponding spherical scatterer are shown in Figure 2.

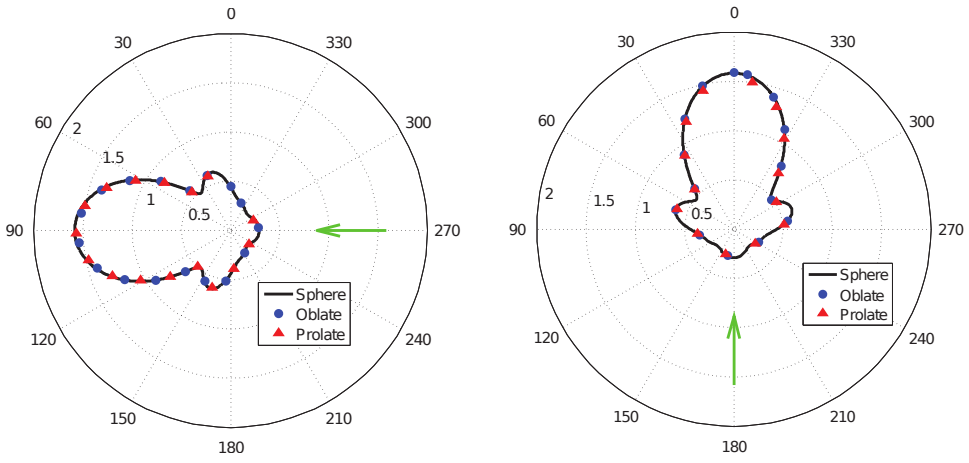

Figure 2: The absolute value of the oblate and prolate far-field scattering amplitude function $|f_\infty|$ tends to the absolute value of the sphere far-field scattering amplitude function when $b \to a$. The $\hat{x}$ incidence (left) and the $\hat{z}$ incidence (right) are shown.

Furthermore, tests were made to verify that the exact solution implemented for a liquid spheroids tends to the known results for impenetrable spheroids, modelling the latter scattererss through extreme density ratios in the former ones. For soft or gas-filled spheroid (or what is equivalent, Dirichlet case) [4, 5, 15], a density ratio $\rho_1/\rho_0 = 1/1000$ was assumed, whereas $\rho_1/\rho_0 = 1000$ was used to evaluate the rigid spheroid (equivalent to

Neumann case) [1, 15]. Computations were made for semi-axis values $a = 1, b = 0.25$ and for an arbitrary incidence angle, $\theta_i = 2\pi/3$. Results are exhibited in Figures 3 and 4. It can be observed there that in the limit of low density contrast, results for both spheroids tend to reproduce the Dirichlet case (Figure 3) while in the limit of high density contrast, they tend to reproduce Neumann case (Figure 4). Moreover, to illustrate intermediate scatterers' types, patterns for moderate density contrasts ($\rho_1/\rho_0 = 3$) are shown.

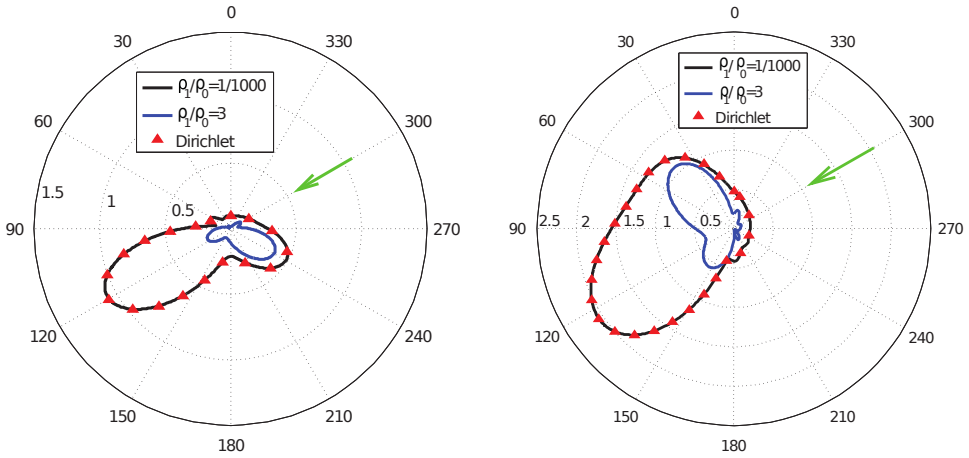

Figure 3: The form function $|f_\infty|$ with two cases of the density ratio and the Dirichlet case. Prolate (left) and oblate (right) cases.

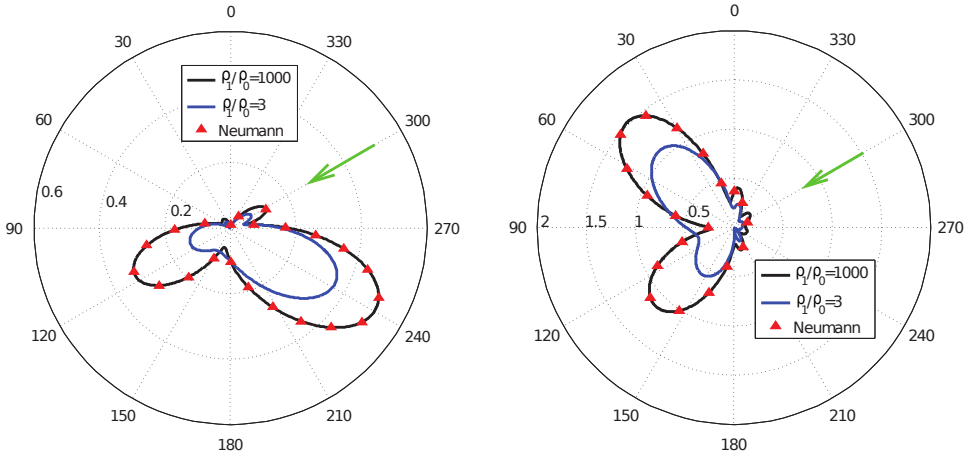

Figure 4: The form function $|f_\infty|$ with two cases of the density ratio and the Neumann case. Prolate (left) and oblate (right) cases.

4.2 Near-field results

Computation of the A_{mn} and B_{mn} coefficients is necessary to obtain the scattered and transmitted acoustic pressures $p_s(\vec{r})$ and $p_t(\vec{r})$ according to Equations (3) and (4).

The total acoustic pressure at a field-point $\vec{r}$ is equal to the the sum of incident and scattered acoustic pressures if $\vec{r}$ is outside the liquid spheroid, or to the transmitted field if $\vec{r}$ is inside it, i. e.

$$p_{total}(\vec{r}) = \begin{cases} p_t(\vec{r}) & \text{if} \quad \xi(\vec{r}) \leq \xi_0 \\ p_{inc}(\vec{r}) + p_s(\vec{r}) & \text{if} \quad \xi(\vec{r}) > \xi_0 \end{cases}$$

Calculations are held for a prolate spheroid with semiaxes $a = 2$, $b = 1$, density ratio $\rho_1/\rho_0 = 1.5$ and wave numbers $k_1 = 1$, $k_0 = 1.5$. Results for the real part of the incident acoustic pressure p_i and the absolute value of total and scattered acoustic pressures are shown in Figure 5 for the Cartesian planes $z = 0$ and $y = 0$. Computed total acoustic pressure verifies the continuity required by the boundary conditions at the interface $\xi = \xi_0$ as it is visually illustrated in Figure 5 (b) and (c).

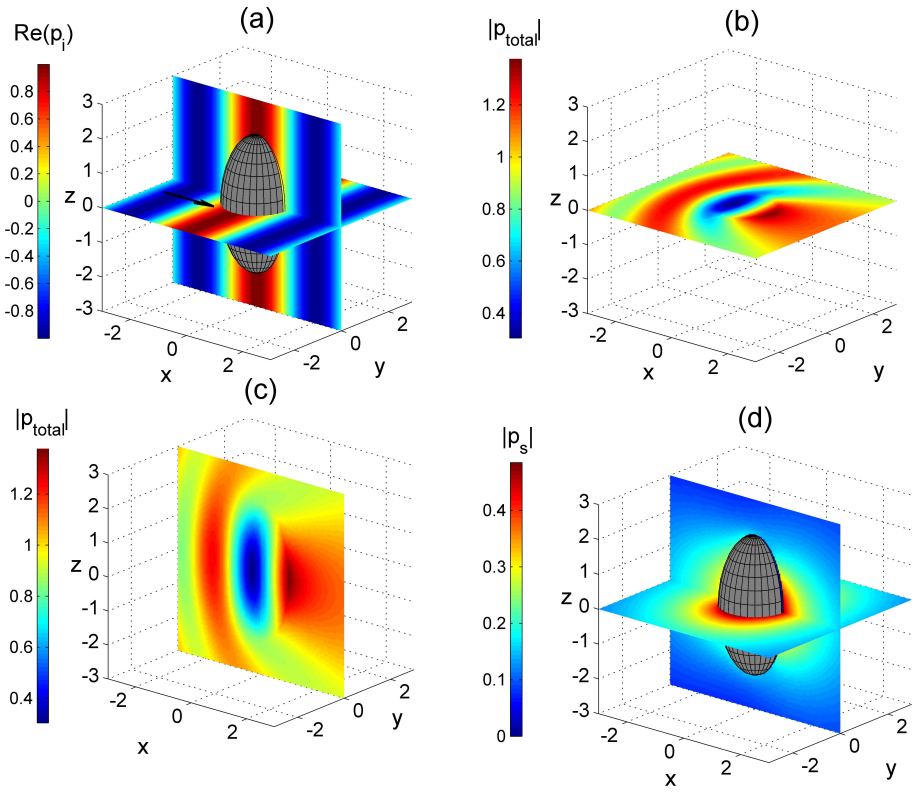

Figure 5: (a) Real part of incident acoustic pressure, $\mathrm{Re}(p_i)$, at the Cartesian planes $z = 0$ and $y = 0$. (b) Absolute value of total acoustic pressure, $|p_{total}|$, at $z = 0$. (c) Absolute value of total acoustic pressure, $|p_{total}|$, at $y = 0$. (d) Absolute value of scattered acoustic pressure, $|p_s|$, at $z = 0$ and $y = 0$. Assumed values: $a = 2$, $b = 1$, density ratio $\rho_1/\rho_0 = 1.5$, wave numbers $k_1 = 1$, $k_0 = 1.5$ and incidence angle $\theta_i = \pi/2$.

4.3 Comparison with reported results

Among the relatively great number of publications addressing the acoustic scattering by penetrable spheroids, such as fluid spheroids inmersed in a fluid surrounding medium, there is an article [11] that reports an analytical solution of the scattered pressure field for $\rho_1/\rho_0 \not\approx 1$, $k_1/k_0 \not\approx 1$ and small values of eccentricity e (i.e. $e = d/(2a) \ll 1$). In that paper a shape perturbation method is used to express the scattered pressure in terms of spherical wave functions, instead of spheroidal ones. Hence, approximate expressions are presented for any value of e as a product of the scattering pressure by a sphere and a polynomial in even powers of e till $\mathcal{O}(e^6)$. Moreover, in that reference some calculated expansion coefficients are presented in a Table for $\rho_1/\rho_0 = 1.22$, $k_0/k_1 = 1.27$ and $a/\lambda_0 = 0.9$, being λ_0 the acoustic wavelength in the medium. Those computed values lead to forward and backscattering cross-sections, σ_f and σ_b, plotted in Figures 5 an 6 of the same paper that can be compared with the corresponding results of the exact solution for $|f_\infty|$, obtained

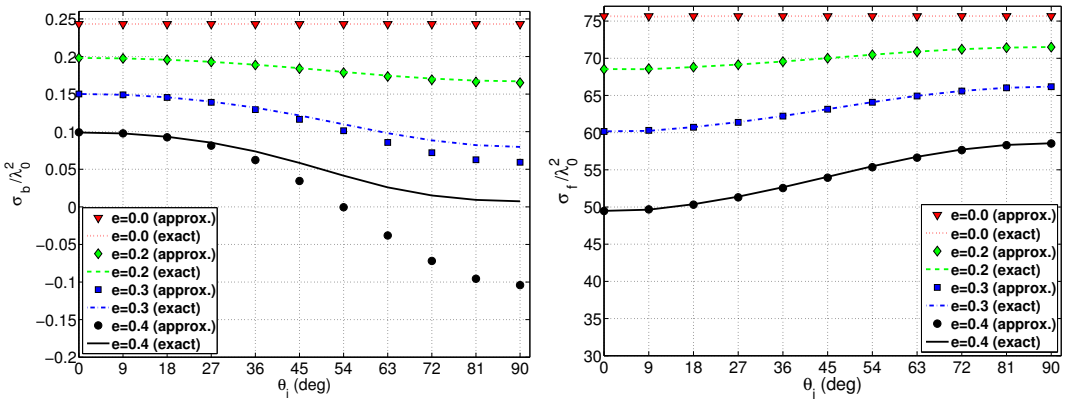

Figure 6: Comparison between exact solution and analytical approximation previously published for prolate spheroids with different kinds of excentricity e. Normalized back-scattering cross section (left) and forward-scattering cross section (right). Both are normalized by λ_0, the wavelength in the medium.

through the codes implemented here for a liquid prolate spheroidal scatterer, given the relationships

$$\sigma_f = 4\pi |f_\infty(\theta_i, \varphi_i)|^2$$
$$\sigma_b = 4\pi |f_\infty(\pi - \theta_i, \varphi_i + \pi)|^2$$

in far-field conditions.

Comparison between normalized backscattering and forward scattering cross-sections (i.e. σ/λ_0^2) predicted by the approximate solution [11] and the exact one computed through the implementation presented here is shown in Figure 6. Good agreement is achieved for the forward scattering case while the agreement gets worse for increasing eccentricity when backscattering is considered. For $e = 0.4$ (i.e. $b/a > 0.9$, which is quite close to be a spherical shape), σ_b takes undesirable negative values at incident angles greater than $54°$, which has no physical sense whereas the exact solution predicts positive values as expected.

5 Routines' sintaxis

The provided routines for far-field patterns computation when plane acoustic waves incide on prolate or oblate spheroids were developed in Julia programming language, which has a MATLAB-like sintaxis, so that MATLAB and Octave users are expected to get easily familiarized with it. They can be freely downloaded from a GitHub repository `https://github.com/elavia/liquid_spheroid` as a ZIP file or as individual files and they can be directly executed from the Julia REPL interface.

The material loaded in the repository is organized in two folders, namely, Linux and Windows, since the routines have been implemented for both operative systems. They were developed and tested in Julia 0.5 under Fedora Linux and in Julia 0.4 under Windows 7, respectively. For ensuring their correct functionality, previous installation of Julia's GSL package (Julia implementation of the GNU Scientific Library) is required[1].

The files `JUL.routines.jl` and `JUL.auxiliar.jl` contain the main and auxiliary functions for the expansion coefficients and the far-field patterns calculations. Several

[1]In most cases it is enough to type `Pkg.add(''GSL'')` at the Julia's prompt.

Julia *scripts* reproducing the results presented in Section 4.1 are also provided. Their names were chosen so that they are related to their particular purpose. Hence, it is not a surprise for example that `script.oblate_liquid.jl` provides the pattern for an oblate spheroid in the liquid case.

The AGD executable files `obl_sphwv` and `pro_sphwv` constitute the *numerical engine* for the calculation of the spheroidal wave functions inside Julia routines and they are called through specialized shell scripts (`.sh` files, under Linux) and batch files (`.bat` files, under Windows). Those executable files were taken from the `scattering-master/spheroidal/sphwv` directory in the AGD software source tree and they can be downloaded from the authors' site at `https://github.com/radelman/scattering`.

For a detailed description of the AGD software and the subtleties in the calculation of spheroidal wave functions, the reader is referred to the original reference that partially inspired this work [15]. The parameters configuration for the AGD software execution inside the Julia routines has been done trough the text files `obl.parameters` and `pro.parameters`. In these files safe values of the parameters were taken in order to ensure reliable results. It is remarkable that input selection associated with extreme cases, such as high frequency, may lead to an unpredicted behaviour, whose comprehension requires deeper understanding of the AGD code. However, these cases are far beyond the scope of this work.

The first step to begin working with the code, once the Julia environment is properly installed, is to download the routines from the authors' repository, uncompress them in a directory and start the Julia REPL interface from that directory. Then, main and auxiliary functions must be loaded at the Julia's prompt through the script `JUL.main.jl`, before any other script is run. Afterwards all the routines are available in the current workspace and can be called from the prompt.

In order to illustrate and clarify the routines' operation, an example session is presented. First, the routines are loaded through the *inclusion* of the main script, i.e.

```
julia > include("JUL.main.jl") ;
```

Therefore, the routines are in the workspace and it is now possible, for example, to calculate the far-field pattern $|f_\infty|$ in the liquid case for a prolate spheroid. This is accomplished with the command

```
julia > include("script.prolate_liquid.jl") ;
```

The pattern is saved in a file called `Out.Pattern.dat` within the current directory. The data format in this file is: angle (in radians) and absolute value of the f_∞ (in arbitrary length units compatible with the ones used for a, b, k). The computing elapsed time is strongly dependent on the computer's speed and the parameters set in the AGD software. All the provided scripts save the results in the same file so that the content is overwritten each time. Scripts output can be plotted with any plotting software (In particular, the plots in this work were made using MATLAB and Gnuplot).

The scripts have a section of user-defined parameters. In the above mentioned example, `script.prolate_liquid.jl` contains

```
# ~~~~~~~~~~~~~~~~~~~~~~~~~~~~~~~~~~~
# User configurable parameters
# ~~~~~~~~~~~~~~~~~~~~~~~~~~~~~~~~~~~
```

```
# Physical parameters
rho10 = 5.00 ; # Density ratio
k_0 = 4 ; # Wave number in media 0
k_1 = 6 ; # Wave number in media 1
a = 1 ; # Major semiaxis spheroid
b = 0.99 ; # Minor semiaxis spheroid
theta_inc = pi/4 ; # Incidence angle (rad)

# Software parameters
M = 8 ;
method = 2 ;
delta_eta = 0.005 ;
```

The meaning of the physical parameters, namely, $\rho_{10}, k_0, k_1, a, b, \theta_i$ is evident from the explicative text after the commentary character `#`. The software parameters section includes parameters related to the spheroidal wave calculation. The `M` parameter is the maximum value taken by m in the coefficients A_{mn}, B_{mn} and is directly associated to the total number of the coefficients to be calculated. For instance, `M` $= 8$ value means a total of $(M+1)(M+2)/2 = 45$ coefficients. The `method` parameter refers to the type of calculation (`method` $= 1$ is convenient for $\xi \gg 1$ and `method` $= 2$ for $\xi \sim 1$). Finally, `delta_eta` is the step on the η-grid and as a consequence of the inequality $-1 \leq \eta \leq 1$, that value leads to a 2/`delta_eta` grid size.

6 Conclusions

A novel implementation of the exact analytical solution for the problem of acoustic scattering by liquid prolate and oblate spheroids governed by Helmholtz equation is presented. A set of computational routines to calculate the expansion coefficients appearing in the mathematical expressions of the scattered and transmitted acoustic pressures is provided. These routines are freely available from the authors' GitHub repository. The coefficients' computation is precisely the most cumbersome task related to numerical calculation of the mathematical expressions above mentioned.

The results predicted by the computational implementation were tested for the geometrical limit when both spheroids, prolate and oblate, tend to the sphere and for the physical limit when they tend to soft or rigid spheroidal scatterers, taking low and high values of dentisities ratios, respectively. In the latter two cases predicted results turn out to be compatible with expected ones for Dirichlet and Neumann boundary conditions.

Additionaly, it has been qualitatively verified, trough the calculation for near-field conditions, that the numerical solution satisfies the boundary condition at the surface of the spheroids. The implemented exact solution has been succesfully compared against a previously reported approximate solution and extended to eccentricity ranges where the approximation does not work properly.

With the aim of generating the provided computational codes, the efficient software by AGD was used in addition to the numerical capabilities of the new scientific programming language Julia. Thus, it was possible to take advantage of the arbitrary floating point precision support in both pieces of code. Furthermore, scripts to reproduce the calculations presented in Section 4.1 are also provided to enable a minimum consistency check.

The developed codes are released intending to contribute with researchers working in acoustic scattering by simplyfing the tedious algorithmic task involved in the resolution of

the cumbersome matricial system when calculating the exact solution for a liquid spheroid scatterer.

Acknowledgements

This work was supported by the PIDDEF Program of the Argentinian Ministry of Defense (13-2014), the Argentinian Navy and the National Council for Scientific and Technical Research (CONICET).

The authors wish to remark once more the outstanding piece of software that Adelman and his collaborators have made freely available to the scientific community. It was a real pleasure to work with it. Of course, the same applies to Julia programming language. Moreover, they acknowledge the work of the programmers' team that have designed and implemented that language. It is marvelous. With both they are in debt.

References

[1] R. Spence and S. Granger, *The scattering of sound from a prolate spheroid*, The Journal of the Acoustical Society of America **23** 701–706, (1951).

[2] A. Silbiger, *Scattering of sound by an elastic prolate spheroid*, The Journal of the Acoustical Society of America **35** 564–570, (1963).

[3] D. S. Burnett, *Radiation boundary conditions for the Helmholtz equation for ellipsoidal, prolate spheroidal, oblate spheroidal and spherical domain boundaries*, Journal of Computational Acoustics 20.04 (2012): 1230001.

[4] M. Furusawa, *Prolate spheroidal models for predicting general trends of fish target strength*, Journal of the Acoustical Society of Japan (E) **9** 13–24, (1988).

[5] I. S. Prario, J. D. Gonzalez, A. Madirolas, S. Blanc, *A Prolate Spheroidal Approach for Fish Target Strength Estimation: Modeling and Measurements*, Acta Acustica united with Acustica 101 **5** 928–940, (2015).

[6] J. M. Jech, J. K. Horne, D. Chu, D. A. Demer, D. T. Francis, N. Gorska, B. Jones et al, *Comparisons among ten models of acoustic backscattering used in aquatic ecosystem research* , The Journal of the Acoustical Society of America **138** 3742–3764, (2015).

[7] C. Yeh, *The diffraction of sound waves by penetrable disks*, Annalen der Physik 468(1-2) 53-61, (1964).

[8] C. Yeh, *Scattering of acoustic waves by a penetrable prolate spheroid. I. Liquid prolate spheroid*, The Journal of the Acoustical Society of America 42(2) 518-521 (1967).

[9] N. Gorska and D. Chu, *Some aspects of sound extinction by zooplankton*, The Journal of the Acoustical Society of America 110(5) 2315-2325, (2001).

[10] Y. Tang, Y. Nishimori and M. Furusawa *The average three-dimensional target strength of fish by spheroid model for sonar surveys*, ICES Journal of Marine Science Journal du Conseil **66** 1176–1183, (2009).

[11] A. D. Kotsis and J. A. Roumeliotis, *Acoustic scattering by a penetrable spheroid*, Acoustical Physics 54 (2), 153-167, (2008).

[12] V. C. Anderson, *Sound scattering from a fluid sphere*, The Journal of the Acoustical Society of America 22 (4) 426–431, (1950).

[13] P.M. Morse and H. Feshbach, *Methods of Theoretical Physics* (McGraw Hill Book Company, New York, 1953).

[14] E. Skudrzyk, *The Foundations of Acoustics* (Springer-Verlag, Berlin, 1970).

[15] R. Adelman, N. A. Gumerov, R. Duraiswami, *Software for Computing the Spheroidal Wave Functions Using Arbitrary Precision Arithmetic*, arXiv:1408.0074v1 [cs.MS], (2014).

[16] J. Bezanson, A. Edelman, S. Karpinski, V. B. Shah, *Julia: A fresh approach to numerical computing*, arXiv:1411.1607v3 [cs.MS] , (2014).

[17] A. L. Van Buren, J. E. Boisvert, *Accurate calculation of prolate spheroidal radial functions of the first kind and their first derivatives*, Quarterly of Applied Mathematics 60 (3) 589–599, (2002).

[18] A. N. Lowan, *Spheroidal Wave Functions* in Handbook of Mathematical Functions, M. Abramovitz and I. A. Stegun [Eds.], 751–759,(Dover Publications Inc. New York, 1972).

[19] C. Flammer, *Spheroidal Wave Functions*, (Standford University press, Standford, California, 1957).

[20] R. Hickling, *Analysis of echoes from a solid elastic sphere in water*, The Journal of the Acoustical Society of America, 34(10), 1582-1592, (1962).